Dalton Transactions

Accepted Manuscript

ROYAL SOCIETY OF CHEMISTRY

www.rsc.org/dalton

Journal Name

ARTICLE

Structural, Electrochemical and Spectroelectrochemical Study on the Geometric and Electronic Structures of [(corrolato)Au^{III}]^{n} (n = 0, +1, −1) Complexes

Received 00th January 20xx,
Accepted 00th January 20xx

DOI: 10.1039/x0xx00000x

www.rsc.org/

Woormileela Sinha,[a] Michael G. Sommer,[b] Margarethe van der Meer,[b] Sebastian Plebst,[c] Biprajit Sarkar,*[b] and Sanjib Kar*[a]

Synthesis of two new Au^{III}corrole complexes with unsymmetrically substituted corrole ligands are presented here. The newly synthesized Au-compounds have been characterized by various spectroscopic techniques. Structural characterization of a representative Au^{III}corrole has also been possible. Electrochemical, UV-vis-NIR/EPR spectroelectrochemical and DFT studies have been used to decipher the electronic structures of various electro-generated species. This is the first UV-vis-NIR/EPR spectroelectrochemical investigations on Au^{III}corroles. Assignment of redox states of electro-generated Au^{III}corroles are supported by DFT analysis. Contrary to the metal centered reduction reported in Au^{III} porphyrins, one electron reduction in Au^{III}corroles have been assigned as corrole centered on the basis of experimental and theoretical studies. Thus, the Au^{III}corroles (not the analogous Au^{III}porphyrin derivatives!) bears a truly redox inactive Au^{III} center. Additionally, these Au-corrole complexes display NIR electrochromism, the origin of which is all on corrole-centered processes.

Introduction

The complexes of gold, the yellow metal, are known to exhibit interesting medicinal properties and have also showed wide range of applications in various catalytic reactions.[1-7] The frequently encountered oxidation states of gold are +I and +III.[8] Gold-porphyrin complexes have been the subject of renewed research interest among the various coordination compounds. These complexes are found to exhibit redox non-innocent gold(III) centers.[9] Ever since the findings of the anti-tumor activity of gold-porphyrin, huge efforts have been devoted to synthesize newer varieties of gold-porphyrin based drugs.[10] Analysis and control of the electron transfer sites in gold-porphyrin complexes are extremely important from the perspectives of their potential applications in molecular electronics and photovoltaic cells.[11-13] Corroles (analogues of porphyrins) have recently gained a lot of interest, because of their unique physical and chemical properties, which are significantly different from the analogous porphyrin macrocycles.[14-42] Owing to the discovery of facile synthetic methodologies,[43-45] the explosive growth of corrole chemistry has thus resulted in the generation of newer and higher oxidation states of metal centers with various exciting implications in catalysis and material sciences.[14-42] Recently, with the silver complexes of corroles we have shown NIR-absorbing properties for the first time in monomeric *meso*-substituted corrole derivatives.[46] Due to the absence of one methine carbon compared to analogous porphyrin derivative, the cavity of corrole is smaller than that of porphyrin and also due to its trianionic nature, corrole always stabilizes metals in formally high oxidation states in comparison to analogous porphyrin species.[14-42] A number of recent literature reports suggest the formation of higher oxidation states of metals in the corrole cavity.[14-42] Of particular interest is the fact that corroles have been shown to stabilize Cr (V), Cr (VI), Fe (IV), Co (V), Ag (III), Cu (III), Cu(IV), etc.[14-42, 46, 47]

In the following, we present the synthesis of two new gold complexes [10-(2,4,5-trimethoxyphenyl)-5,15-bis(4-cyanophenyl)corrolato-Au(III)], **1**, and [10-(4,7-dimethoxynaphthalen-1-yl)-5,15-bis(4-cyanophenyl)corrolato-Au(III)], **2** with corrolato ligands that are unsymmetrically substituted (Scheme 1). We also present structural characterization, electrochemical, UV/vis/NIR-EPR spectroelectrochemical, and DFT approaches to address the composition of the redox series on oxidation and reduction of the native gold (III) corroles. Additionally, we compare these systems to their Cu- and Ag-analogues and address the issue of NIR-electrochromism in these complexes.

[a]*School of Chemical Sciences, National Institute of Science Education and Research (NISER), Bhubaneswar – 751005, India, E-mail: sanjib@niser.ac.in*
[b]*Institut für Chemie und Biochemie, Anorganische Chemie, Fabeckstraße 34-36, D-14195, Berlin, Germany, E-mail: biprajit.sarkar@fu-berlin.de*
[c]*Institut für Anorganische Chemie, Universität Stuttgart, Pfaffenwaldring 55, D-70569, Stuttgart, Germany*

Electronic Supplementary Information (ESI) available: Crystallographic data and packing diagram for **2**. UV–Vis., ESI-MS data, NMR data, electrochemical data, and X-band EPR data, Change in the UV-Vis spectrum of **2**, **2**$^{+}$, and **2**$^{-}$. TD-DFT calculated absorption spectra for **1**, **1**$^{+}$, **1**$^{-}$, **2**, **2**$^{+}$, and **2**$^{-}$, ORTEP diagram of **2**. CCDC 1409235 contains the supplementary crystallographic data for **2**. These data can be obtained free of charge via www.ccdc.cam.ac.uk/data_request/cif.

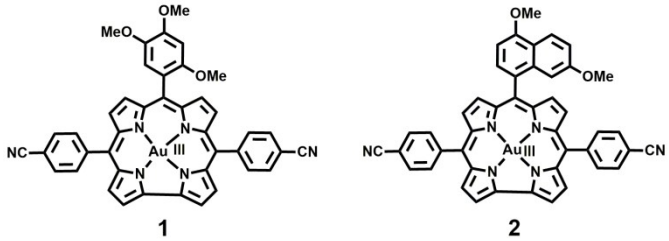

Scheme 1 Structures of the gold(III) corrole complexes [10-(2,4,5-trimethoxyphenyl)-5,15-bis(4-cyanophenyl)corrolato-Au(III)], **1**, and [10-(4,7-dimethoxynaphthalen-1-yl)-5,15-bis(4-cyanophenyl)corrolato-Au(III)], **2**.

Results and discussion

Synthesis and characterization

The gold(III) corrole complexes were synthesized by slight variation of a procedure demonstrated by Thomas et al.[48] The respective free-base corroles in pyridine were treated with a little excess of gold(III) acetate for about an hour. After evaporation of the solvent, chromatographic separation and subsequent recrystallization pure crystalline gold(III) corrole complexes, **1** and **2** were obtained. The identification and characterization of the synthesized complexes were performed by elemental analysis, mass spectroscopy, ^{1}H NMR, UV-visible spectroscopy and single-crystal X-ray diffraction analysis (see ESI). ESI mass spectral analysis indicated the existences of peaks at m/z = 860.6794 corresponding to $[\mathbf{1}]^+$ and *m/z* = 880.1810 corresponding to $[\mathbf{2}]^+$ respectively (Fig. S1, ESI†).

NMR spectra

Similar to the lighter analogues of the coinage metal series, ^{1}H NMR spectra of the synthesized gold(III) corrole complexes also exhibit sharp resonances.[48-50] All the eighteen aromatic protons are clearly visible from the distinct signals of ^{1}H NMR spectrum of **1** in the diamagnetic region (Fig. S2, ESI†). The β-pyrrolic protons of **1** appear as doublets in the region of 9.20-8.80 ppm with the characteristic coupling constant of *J*~4.7 Hz.[49, 50] The remaining ten aromatic protons appear in the region of 8.40-7.01 ppm. Three sharp singlets in the region of 4.21-3.60 ppm correspond to the three different sets of methoxy protons of **1**. Clearly resolved four sets of doublets in the region 9.17-8.64 ppm correspond to the eight β-pyrrolic protons of the macrocycle skeleton in **2** (Fig. S3, ESI†). The rest of the thirteen aromatic protons, i.e. the *meso*-aryl protons resonate in the span 8.50-6.40 ppm. Two sets of methoxy groups in **2** appear as singlets at 4.27 ppm and 2.97 ppm. ^{13}C NMR spectral analysis of **2** reveals twenty-eight signals, lesser than the total number of carbons, due to some symmetry of the molecule (Fig. S4, ESI†).

Crystal Structure

Needle-like single crystals of **2** were obtained from a solution of dichloromethane and benzene. The crystallographic data has been tabulated in Table S1 (ESI†). The gold(III) corrole complex **2** crystallized as two molecules along with two molecules of benzene solvent in the unit cell of triclinic P-1 space group. Gold fits almost perfectly in the macrocyclic framework with a very slight elevation of 0.0042 Å from the N4 plane (Fig. 1). The geometry around the gold atom is however not perfectly square planar due to the

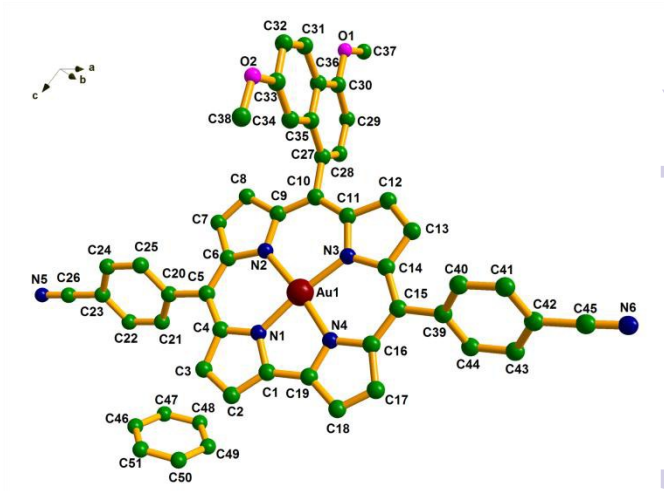

Fig. 1 Single-crystal X-ray structure of **2**.

unequal bite angles of 91.68°, 95.60°, 91.91° and 80.81° for the N1-Au-N2, N2-Au-N3, N3-Au-N4 and N4-Au-N1 bonds respectively (Fig. S5, ESI†). The M-N bond distances are longer in case of the gold(III) corrole, **2** in comparison with the silver complexes for the same ligand system as anticipated.[46-50] The M-N bond distances range from 1.96 Å for Au-N3 to 1.93 Å for Au-N1 bonds. The complete planarity of the macrocyclic backbone is disturbed due to the deviation of the pyrrolic rings with angles of -0.0742 Å (N4) and 0.0984 Å(N2) from the mean corrole plane. The substituted phenyl rings at C-5 and C-15 and the naphthyl- substituent at C-10 positions make angles of 48.30°, 51.37° and 82.19° with reference to the mean corrole plane. Thus the naphthyl-substituent stands almost perpendicular to the mean corrole plane of complex, **2**.

In case of the lightest congener of the coinage metal series, Cu, by using the same ligand framework, a deviation of 0.0301 Å of the central copper atom from the N4 plane has been observed.[47] The observed saddling of the corrole ligand framework has been further explained on the basis of electron transfer from cor^{3-} ligand to the empty d_{x2-y2} orbital of Cu (III) center.[47] In case of Ag, the observed deviation was ~0.0194 Å.[46] Thus it can be assumed that the saddling effect decreases pronouncedly as we go down the group (Cu→Ag→Au). X-ray analysis thus indicates negligible saddling in the Au-corrole complexes and hence suggests their redox innocence nature, i.e the presence of truly Au (III) centers in the native state.

The molecules of **2** are packed in such a manner that two of such molecules form a pair stabilized by π–π stacking interaction (Fig. S6, ESI†). The distance between the two metal centers in a pair is 4.6798 Å. These pairs of molecules appear along parallel lines. In each pair the molecules are oriented in such a way so that the bulky naphthyl substituents at C-10 positions are placed furthest away to avoid steric crowding. The closest distance between any two metal centers of two such pairs is 5.1713 Å. The mean plane separation can be considered to be 3.51 Å. Thus, strong parallely displaced π-π interaction help in the stacking of the macrocycles.

Redox properties of 1 and 2

The cyclic voltammetric and differential pulse voltammetric studies

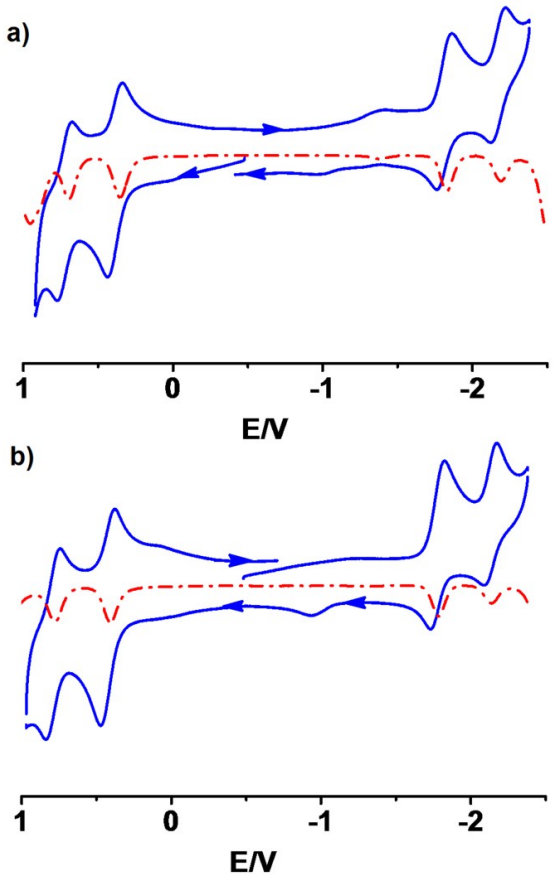

Fig. 2 Cyclic voltammograms (————) and differential pulse voltammograms (-·-·-·-·) of a) **1** and b) **2**. The potentials are vs. ferrocene/ferrocenium.

for the gold(III) corrole complexes, **1** and **2** were performed in dichloromethane using 0.1 M TBAP as the supporting electrolyte. Both the complexes displayed two successive oxidative and two reductive reversible couples *versus* ferrocene/ferrocenium (Fig. 2, Table S2, ESI†). The first oxidative process was recorded at E^0_{298}, V (ΔEp, mV): 0.39(70) and 0.42(70) for **1** and **2** respectively. The second oxidative couple was observed at E^0_{298}, V (ΔEp, mV): 0.72 (80) and 0.79 (80) for **1** and **2** respectively. The first reduction appeared at E^0_{298}, V (ΔEp, mV): -1.81(80) and -1.78(80) in case of **1** and **2** respectively. The second reductive process was observed at E^0_{298}, V (ΔEp, mV): -2.17(80) and -2.13(80) in case of **1** and **2** respectively. Thus, is it seen, that the redox potentials for the two Au-corrole complexes are virtually identical. However, some intriguing trends are observed on comparing the redox potentials of display only one reduction step,[46] whereas the present Au-complexes display two reversible reduction steps. Furthermore, the these complexes with their analogous Ag-complexes.[46] The oxidation potentials for the Au- and Ag-complexes are in very similar ranges. The reductive electrochemistry however shows quite a few differences for the two sets of complexes. The Ag-complexes potentials for the reduction steps are shifted to the negative side for the Au-complexes in comparison to their Ag-analogues.[46] These trends are already an indication of similar locus of oxidation for both types of complexes, but likely different locus of reduction for the Ag- and Au-complexes. To procure detailed knowledge about the reversibility of the redox processes in these complexes and to get a deeper insight into the electronic structures of the electrooxidized and electroreduced species of these complexes, UV-vis-NIR and EPR spectroelectrochemical studies were carried out. DFT and TD-DFT calculations were also done for further confirmation.

EPR spectroelectrochemistry and spin density calculations

In the quest for re-confirmation of the diamagnetic character of the gold(III) corrole complexes and also to ascertain the actual reversibility of the redox processes in those complexes, EPR experiments for the one-electron oxidised and one-electron reduced forms of both **1** and **2** were performed. In the native state both the complexes (**1** and **2**) do not show any characteristic EPR signal as is expected for the tetra coordinated square planar gold (III) complexes with $5d^8$ electronic configuration.[8] X-band EPR spectroscopic results of the oxidised and reduced forms in either of the designed gold(III) corrole complexes have very similar pattern, thus one of them has been discussed here in details. The *in-situ* generated one-electron oxidized species $(\mathbf{1})^{\bullet+}$ in CH_2Cl_2/0.1 M Bu_4NPF_6 displays a typical ligand based EPR spectrum (Fig. 3). The sharp EPR signal with experimentally obtained *g* value of 2.005 for the one electron oxidized species, $(\mathbf{1})^{\bullet+}$, its appearance in fluid solutions at ambient temperatures, and the narrow total width of the signal clearly point towards a corrole centered signal.[46] The calculated *g* value by using B3LYP/def2- TZVP level of theory are g_1 = 1.992; g_2 = 1.996; g_3 = 2.003 (Table 1). The theoretically calculated *g*-values are thus consistent with the experimentally obtained ones. The extremely small *g*-anisotropy predicted by theory is not

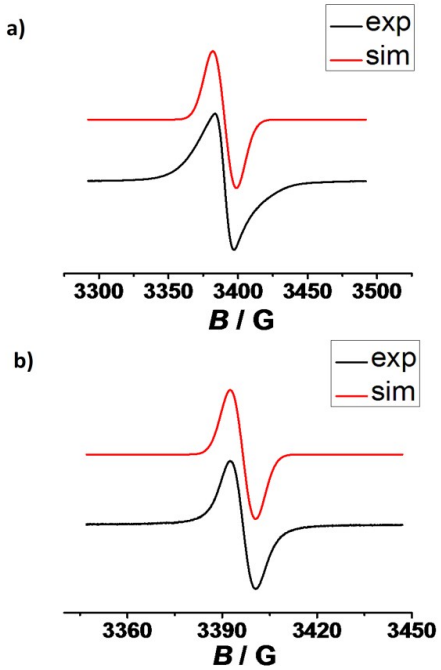

Fig. 3 X-band EPR spectrum of a) $(\mathbf{1})^{\bullet+}$ with simulation and b) $(\mathbf{1})^{\bullet-}$ generated by in-situ electrolysis at 295 K in CH_2Cl_2/0.1 M Bu_4NPF_6.

resolved in the experimental spectrum under X-band conditions. Similar spectral signature has been also observed for $(\mathbf{2})^{\bullet+}$ (Fig. S7, ESI†, Table 1). Spin-density calculations of the two gold(III) complexes were carried out. The Löwdin population analysis of both $(\mathbf{1})^{\bullet+}$ and $(\mathbf{2})^{\bullet+}$ reveal that the unpaired spin is predominantly localized on the corrole ligands with only ~1% residing on the central Au atoms in both the complexes (Fig. 4, Table 2). More specifically the spin resides mainly at the *meso*-carbons C-5, C-10 and C-15 and also considerable contributions exist from two of the donor nitrogen atoms as can be seen in the Fig. 4. Such distribution of spin is in contrary to our previously investigated one electron oxidized Cu-corrole species where 44% spin density was found on the Cu atoms.[47] This spin distribution is however, in line with our previous study on one electron oxidized Ag-corroles where only <1% spin density resided over Ag atoms.[46] Thus, similar to the assignment performed on the oxidized Ag-corroles,[46] for the one electron oxidized Au-corroles, a formulation of $[(\text{corrolato}^{\bullet 2-})\text{Au}^{\text{III}}]^{\bullet+}$ will be best suited for the one- electron oxidized species.

The *in-situ* generated one-electron reduced species $(\mathbf{1})^{\bullet-}$ in CH_2Cl_2/0.1 M Bu_4NPF_6 displays an isotropic EPR spectrum in fluid solutions with a *g*-value of 1.995 (Fig. 3). The calculated *g* values by using B3LYP/def2-TZVP level of theory are g_1 =1.951; g_2 = 2.008; g_3 = 2.013. Similar to the one-electron oxidized species, the small *g*-anisotropy predicted by theory was not resolved in the experimental spectrum. The EPR spectrum of $(\mathbf{2})^{\bullet-}$ has very similar features to the one discussed above (Fig. S7, ESI†). The analogous gold(III) porphyrin complex exhibited the generation of Au^{II} species on one electron reduction which was authenticated by the appearance of a broad signal in the EPR spectrum and the corresponding *g* values were found to be g_1 = 2.182; g_2 = 2.043; g_3 = 1.979.[51] Contrary to it, gold-corroles as reported in this demonstration, on one electron reduction, results in the formation of gold(III)-corrole π–anion radical exclusively.

Löwdin spin density calculations on $(\mathbf{1})^{\bullet-}$ as well as $(\mathbf{2})^{\bullet-}$ demonstrate almost entirely ligand centered spin with only 0.1% contribution from the central Au atom. The major contributions are observed from the *meso* carbons C-5 and C-15 and also from the alternate carbon atoms at the periphery of the macrocyclic skeletons in both $(\mathbf{1})^{\bullet-}$ and $(\mathbf{2})^{\bullet-}$(Fig. 4, Table 2). Such kind of spin distribution differs completely to our earlier observations on one electron reduced species of copper and silver corroles with similar kind of ligand frameworks.[46, 47] For the analogous Cu- and Ag-complexes, EPR spectroscopy together with DFT calculations had clearly shown the generation of Cu^{II} and Ag^{II} on one-electron reduction of the corresponding Cu^{III}/Ag^{III}-corrole complexes. Thus, the DFT calculations along with the EPR studies unambiguously point towards the major contribution of $[(\text{corrolato}^{\bullet 4-})\text{Au}^{\text{III}}]^{\bullet-}$ form to the one-electron reduced species of these complexes.

Table 1 EPR data[a] of paramagnetic states[b]

Complex	*g* value exp	*g* values B3LYP/def2-TZVP
$\mathbf{1}^{\bullet+}$	2.005	g_1 = 1.992; g_2 = 1.996; g_3 = 2.003
$\mathbf{2}^{\bullet+}$	1.982	g_1= 1.993; g_2= 1.996; g_3= 2.003
$\mathbf{1}^{\bullet-}$	1.995	g_1 =1.951; g_2= 2.008; g_3= 2.013
$\mathbf{2}^{\bullet-}$	1.997	g_1= 1.952; g_2= 2.009; g_3= 2.012

[a] *g* values measured at 295 K. [b] From EPR spectroelectrochemistry in CH_2Cl_2/0.1 M Bu_4NPF_6.

Table 2 DFT (B3LYP/def2-TZVP) calculated Löwdin spin densities on Au

Complex	Au
$\mathbf{1}^{+}$	1.1 %
$\mathbf{1}^{-}$	0.1 %
$\mathbf{2}^{+}$	1.0 %
$\mathbf{2}^{-}$	0.1 %

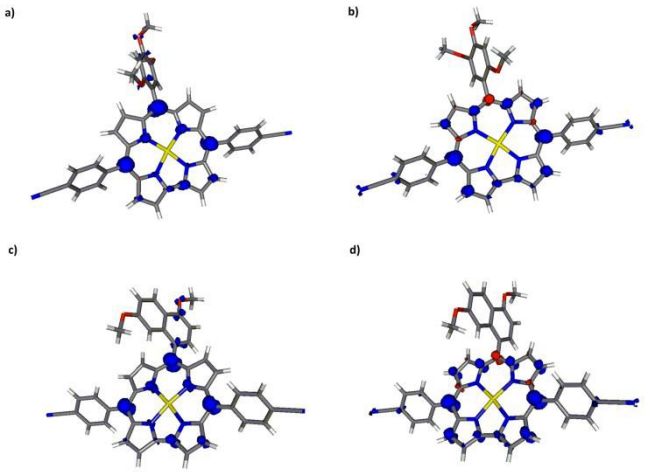

Fig. 4 Spin density representations for a) $\mathbf{1}^{\bullet+}$, b) $\mathbf{1}^{\bullet-}$, c) $\mathbf{2}^{\bullet+}$ and d) $\mathbf{2}^{\bullet-}$. (iso-value 0.005).

UV-vis-NIR spectroelectrochemistry, NIR electrochromism and TD-DFT calculations

As the absorption spectra of both the Au-corroles are almost identical in all the possible redox states, only one of them will be discussed here in detail (Table 3 and Fig. 5). In the native state both the Au-complexes exhibit very similar spectral pattern with Soret bands at 422–424 nm and other major bands at 572–574 nm (Fig. S8 and Fig. S9, ESI†). The peak positions and intensity can be corroborated with other previously reported Au-corroles.[48-50] The origin of all the bands in the neutral Au-corroles has been assigned with the help of TD-DFT calculations (Table 4, and Fig. 6). The TD-DFT calculations clearly show that the origins of these bands are all from either intra-ligand transitions, or intra-ligand charge transfer (ILCT) transitions. The orbitals from the metal center do not contribute to any of these bands (Fig. S10-S15, ESI†).

On one-electron reduction of **1** to $(\mathbf{1})^{\bullet-}$, all the bands in the visible region are reduced in intensity (Fig. 5c). The Soret band is slightly blue shifted and is almost found to disappear. The other low intensity bands also disappear and a new band appears at 668 nm. Contributions from the HOMOβ→LUMOβ, HOMOβ→LUMO+1β, HOMO-1α→LUMOα, HOMOβ→LUMO+1β were determined for this new transition (Table 5, Fig. 7). TD-DFT

explains the origin of this 668 nm band to be of intra ligand charge transfer (ILCT) transition in nature. An additional weak band at 803 nm also has a similar origin. TD-DFT calculations predict a very weak band which is further lower in energy. We have not been able to experimentally determine such a band. Upon one-electron reduction, the metal centers in the native state, i.e. the Au(III), are not reduced and this observation is in contrary to the previously reported Au-porphyrins, Cu-corroles and Ag-corroles (Scheme 2).[46, 47, 51] In case of Cu/Ag-corroles, on one-electron reduction the metal to ligand charge transfer (MLCT) transitions were detected (Scheme 2), however this kind of MLCT transitions are absent in Au-corroles.

On one electron-oxidation of gold(III)-corroles, all the bands in the visible region are reduced in intensity and are slightly blue shifted. However, the most characteristic feature is the appearance of a long wavelength band in the NIR region at 1350 nm for $(\mathbf{1})^{\bullet+}$ (Table 3, Fig. 5a). Such appearance of NIR bands were also observed on oxidation of the previously reported copper(III)/silver(III)corroles.[46, 47] The appearance of this long wavelength bands in the NIR region on one electron-oxidation of **1** and **2** are unique in nature and have never been observed before for the previously reported monomeric gold(III)-corroles or gold(III)-porphyrin derivatives.[48-51]

Origin of these new bands at the NIR regions for $(\mathbf{1})^{\bullet+}$ and $(\mathbf{2})^{\bullet+}$ can be explained with the help of TD-DFT calculations and are assigned to be the contributions from HOMO-1β→LUMOβ orbitals (Table 6, Fig. 8). Intra ligand charge transfer (ILCT) transitions are responsible for the origin of these NIR-bands. On further oxidation to $\mathbf{1}^{2+}$, all the bands in the visible region are reduced in intensity,

Table 3 UV–vis–NIR data of **1** and **2** from spectroelectrochemistry[a]

Complexes	λ_{max} [nm] (ε [10^3 $M^{-1}cm^{-1}$])
$\mathbf{1}^0$	331 (15.1); 423 (136.4); 493 (3.3); 534 (10.2); 574 (41.6)
$\mathbf{1}^-$	389 (sh); 421 (32.8); 584 (10.3); 668 (14.3); 803 (sh)
$\mathbf{1}^+$	328 (12.5); 405 (sh); 420 (67.8); 457 (sh); 538 (12.3); 565 (11.8); 636 (sh); 690 (sh); 1350 (1.3)
$\mathbf{1}^{2+}$	291 (21.1); 408 (59.8); 522 (sh); 690 (sh); 1200 (5.9)
$\mathbf{2}^0$	333 (14.3); 424 (121); 494 (3.6); 534 (9.0); 573 (37.0)
$\mathbf{2}^-$	336 (19.4); 395 (sh); 425 (46.1); 493 (sh); 525 (h); 578 (10.9); 670 (17.9); 810 (sh)
$\mathbf{2}^+$	331 (12.2); 401 (55.2); 421 (56.1); 455 (sh); 536 (9.5); 572 (7.6); 678 (sh); 1350 (4.0)

[a]Measurements in CH_2Cl_2/0.1 M Bu_4NPF_6 (OTTLE spectroelectrochemistry).

Table 4 TD-DFT calculated electronic transitions for **1**

Comp	Main contributing excitation (%)	Transition wavelength (nm)	Oscillator strength	Exp. transition wavelength (nm)	Molar absorption coefficient, $M^{-1}cm^{-1}$
1	HOMO-1→ LUMO+1(24) HOMO → LUMO(72)	530	0.292	534/574	10200/41600
	HOMO → LUMO+1(30) HOMO → LUMO+2(34)	427	0.215	423/493	136400/3300
	HOMO-1→ LUMO+1(34) HOMO → LUMO+3(47)	421	0.845		

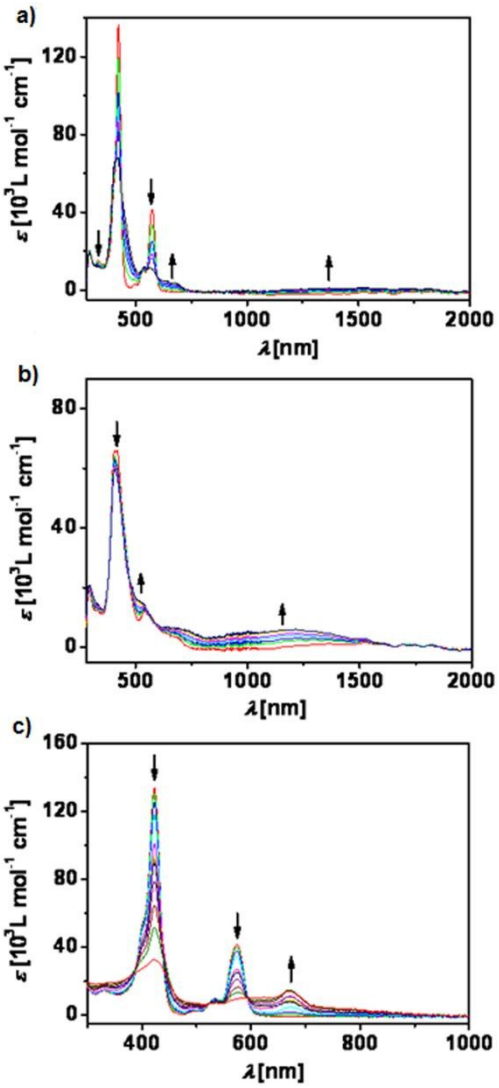

Fig. 5 Change in the UV-vis spectrum of **1** during a) first oxidation, b) second oxidation and c) first reduction. Result from OTTLE spectroelectrochemistry in CH_2Cl_2/0.1 M Bu_4NPF_6.

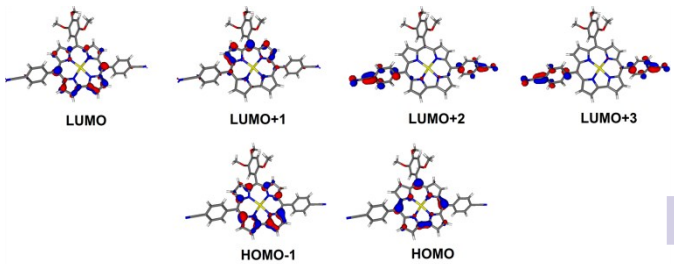

Fig. 6 Composition of selected molecular orbital of **1**.

Table 5 TD-DFT calculated electronic transitions for $\mathbf{1}^-$

Comp	Main contributing excitation (%)	Transition wavelength (nm)	Oscillator strength	Exp. transition wavelength (nm)	Molar absorption coefficient, $M^{-1}cm^{-1}$
$\mathbf{1}^-$	HOMOα→ LUMOα(89)	1761	0.100	not observed	
	HOMOα→ LUMO+2α(88)	911	0.217	803	sh
	HOMOβ→ LUMOβ(47) HOMOβ→ LUMO+1β(23)	654	0.237	668	14300
	HOMO-1α→ LUMOα(17) HOMOβ→ LUMOβ(32) HOMOβ→ LUMO+1β(34)	653	0.162		
	HOMO-1α→ LUMOα(47) HOMOβ→ LUMO+1β(30)	468	0.194	421	32800
	HOMO-2α→ LUMOα(16) HOMOβ→ LUMO+4β(33)	441	0.407		
	HOMO-1α→ LUMO+1α(41)	429	0.532		

Table 6 TD-DFT calculated electronic transitions for $\mathbf{1}^+$

Comp	Main contributing excitation (%)	Transition wavelentgth (nm)	Oscillator strength	Exp. transition wavelength (nm)	Molar absorption coefficient, $M^{-1}cm^{-1}$
$\mathbf{1}^+$	HOMO-1β→ LUMOβ(94)	1521	0.109	1350	1300
	HOMO-2β→ LUMOβ(92)	959	0.034		
	HOMO-7β→ LUMOβ(34) HOMO-5β→ LUMOβ(38)	604	0.062	636	sh
	HOMO-7β→ LUMOβ(54)	562	0.111	538/ 564	12300/ 11800
	HOMOα→ LUMO+1α(68)	557	0.080		
	HOMO-1α→ LUMO+1α(31) HOMO-5β→ LUMOβ(18) HOMOβ→ LUMO+2β(26)	521	0.161		
	HOMO-1β→ LUMO+2β(48)	438	0.167	405/420/ 457	sh/67800 / sh
	HOMO-3α→ LUMOα(73)	427	0.101		

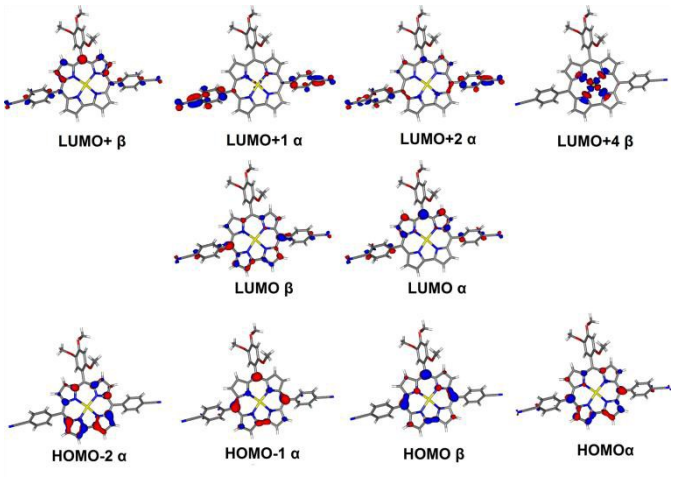

Fig. 7 Composition of selected molecular orbitals of $\mathbf{1}^-$.

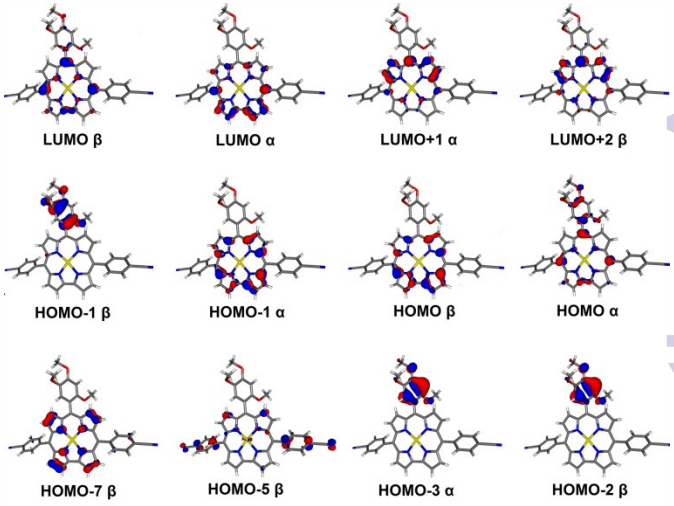

Fig. 8 Compositions of selected molecular orbitals of $\mathbf{1}^+$.

however the near IR band is found to gain some more intensity around 1200 nm (Fig. 5b). A doubly oxidized corrole core, will lead to enhancement in ILCT transitions, and this is what is experimentally observed for the two-electron oxidized species. On reversing the potential back to the starting potential, the bands in the NIR region disappear completely, and the bands in the visible region are restored to their original intensity. These complexes thus display electrochromism in the NIR region. The absorptions in the NIR region can be turned on and off by reversible electron transfer steps. The origin of all these redox steps and transitions are on the corrole ligands. Due to the lack of stability of the species $\mathbf{2}^{2+}$ within the time-scale of the spectroelectrochemistry measurements, the spectral pattern on second oxidation could not be generated in case of **2**. Furthermore, the second reduction step for both complexes turned out to be irreversible in the spectroelectrochemical measurements, and hence those spectra have not been discussed here.

Conclusions

In summary, we have presented here the synthesis of two Au-corrole complexes, a thorough spectroscopic and electrochemical

characterization of both, and single crystal X-ray diffraction studies on one of the complexes. The electronic structures of both Au-corrole complexes have been investigated in the accessible redox states, and comparisons have been made with the Cu-and Ag-analogues. This work serves as the first such study on the spectroelectrochemical characterization of the various redox forms of the corrolato-gold complexes. With a combination of EPR, DFT calculations and UV-vis-NIR spectroelectrochemical measurements, conclusions have been drawn on the site of electron transfer and the nature of electronic transitions on electro oxidation and electro reduction of the corrolato-gold complexes. In both the cases of oxidation and reduction it has been concluded that the redox processes are solely corrole ring-based in nature. Thus, the metal centre remains completely innocent in both the cases, contrary to what has been observed in case of Au^{III} porphyrins, Cu^{III}corroles and Ag^{III}corroles.

In a simplified model, the ligand field strength in the case of Au^{III}-corrole complexes will be larger than their Cu^{III}/Ag^{III}-corroles as well as Au^{III}-porphyrin counterparts. While the former is an effect of intrinsic lower ligand field strengths for a 3d/4d metal compared to a 5d metal center, the latter is an effect of a weaker ligand field for a porphyrin ligand compared to its corrole counterpart. The effect of a large ligand field on Au-corrole complex will destabilize the d_{x2-y2} orbital in a square planar environment and push it to such higher energy, that it becomes inaccessible for the reduction steps. For Au-porphyrin as well as for Cu/Ag-corrole complexes, the d_{x2-y2} orbital is still energetically accessible due to lower ligand field strengths as discussed above. The net result of all these effects is thus metal centered reduction for the Cu^{III}/Ag^{III}-corroles and the Au^{III}-porphyrin complexes, and a corrole centered reduction for the Au^{III}-corrole complexes. The oxidation steps for all three types of complexes are ligand centered, a result that is a consequence of the inaccessibility/instability of Au^{IV} for these complexes. The above results can be summarized as follows:

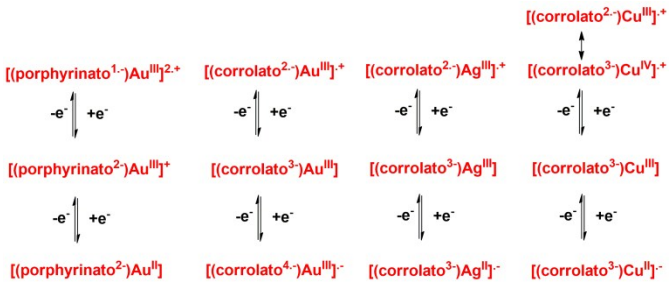

Scheme 2 Formal oxidation state distributions for the various redox states in porphyrinato-gold complexes (extreme left),[51] corrolato-gold complexes (2nd from left), and corrolato-silver complexes (2nd from right),[46] and corrolato-copper complexes (extreme right).[47]

We have also shown here that such Au-corrole complexes can display NIR-electrochromism where the origin of all redox and absorption processes are ligand centered. Considering the square planar geometry of these metal complexes, it should be easy to deposit them on electrode surfaces with an aim of potentially generating smart windows. We note once more, that all redox process discussed for the complexes above are corrole centered, thus proving once again its non-innocent character.

Experimental Section

Materials

The precursors pyrrole, p-chloranil, 4-Cyano benzaldehyde, 2,4,5-Trimethoxy benzaldehyde, 4,7-Dimethoxy naphthaldehyde and TBAP (Tetrabutyl ammonium perchlorate) were purchased from Aldrich, USA. Gold(III) acetate was purchased from Alfa Aeser. Other chemicals were of reagent grade. Hexane and CH_2Cl_2 were distilled from KOH and CaH_2 respectively. For spectroscopy and electrochemical studies HPLC grade solvents were used.

Physical measurements

UV–Vis spectral studies were performed on a Perkin–Elmer LAMBDA-750 spectrophotometer. The elemental analyses were carried out with a Perkin–Elmer 240C elemental analyzer. The NMR measurements were carried out using a Bruker AVANCE 400 NMR spectrometer. Chemical shifts are expressed in parts per million (ppm) relative to residual chloroform (δ = 7.26). Electrospray mass spectra were recorded on a Bruker Micro TOF–QII mass spectrometer. Cyclic voltammetry measurements were carried out using a CH Instruments model CHI1120A electrochemistry system. A glassy–carbon working electrode, a platinum wire as an auxiliary electrode and a saturated calomel reference electrode (SCE) were used in a three–electrode configuration. Tetrabutyl ammonium perchlorate (TBAP) was the supporting electrolyte (0.1M) and the concentration of the solution was 10^{-3} M with respect to the complex. The half wave potential E^0_{298} was set equal to 0.5(Epa + Epc), where Epa and Epc are anodic and cathodic cyclic voltammetric peak potentials, respectively. The scan rate used was 100 mV s^{-1}. EPR spectra in the X band were recorded with a Bruker System EMX. Simulations of EPR spectra were done using the Simfonia program. UV-vis-NIR absorption spectra were recorded on an Avantes spectrometer system: Ava Light-DH-BAL (light source), AvaSpec-ULS2048 (UV-vis-detector) and AvaSpec-NIR256-2.5TEC (NIR-detector). Spectroelectrochemical measurements were carried out using an optically transparent thin layer electrochemical (OTTLE) cell.[52]

Crystal structure determination

Needle-like single crystals of **2** were developed by slow diffusion of a solution of the **2** in dichloromethane into benzene, followed by slow evaporation under atmospheric conditions. The crystal data of **2** were collected on a Bruker Kappa APEX II CCD diffractometer at 100 K. Selected data collection parameters and other crystallographic results are summarized in Table S1. All data were corrected for Lorentz polarization and absorption effects. The program package SHELXTL[53] was used for structure solution and full matrix least squares refinement on F2. Hydrogen atoms were included in the refinement using the riding model. Contributions of H atoms for the water molecules were included but were not fixed. Disordered solvent molecules were taken out using SQUEEZE command in PLATON.[54] CCDC1409235 contains the supporting

crystallographic data for **2**. These data can be obtained free of charge via www.ccdc.cam.ac.uk/data_request/cif.

Computational details

DFT calculations were done with the ORCA 3.0.0 program[55] package using the BP86 and B3LYP functional for the geometry optimization and single-point calculations respectively.[56-58] The restricted and unrestricted DFT methods were employed for closed and open shell molecules respectively. All calculations were run with empirical Van der Waals correction (D3).[59] Convergence criteria were set to default for the geometry-optimizations (OPT) and tight for SCF calculations (TIGHTSCF). Relativistic effects were included with the zeroth-order relativistic approximation (ZORA).[60] Triple-ζ-valence basis sets (TZVPP-ZORA)[61] were employed for all atoms. Calculations were performed using the resolution of the identity approximation[62-65] with matching auxiliary basis sets. Low-lying excitation energies were calculated with time-dependent DFT (TD-DFT). Solvent effects were taken into account with the conductor-like screening model (COSMO)[66, 67] for all calculations. Spin densities were calculated according to the Löwdin population analysis.[68] Molecular orbitals and spin densities were visualized with the Molekel 5.4.0.8 program.[69]

Synthesis of 10-(2,4,5-Trimethoxyphenyl)-5,15-bis(4-cyanophenyl)corrolato-Au(III), 1

1 was prepared after slight modifications of the procedure reported by Thomas et al.[48] A mixture of 10-(2,4,5-Trimethoxyphenyl)-5,15-bis(4-cyanophenyl) corrole (0.050 gm, 0.075 mmol) and an excess of gold acetate (0.140 gm, 0.375 mmol) was dissolved in 5 mL of pyridine under stirring condition. After an hour, the solvent was evaporated and the red-brown colored crude product was subjected to column chromatography using silica gel (100-200 mesh) and dichloromethane as eluent. The desired compound was collected as a bright-red fraction. Upon recrystallization (CH_2Cl_2/hexane) pure crystalline compound, **1** was obtained. Yield: 30% (20mg). Anal. Calcd (found) for $C_{42}H_{27}AuN_6O_3$ (**1**): C, 58.61 (58.43); H, 3.16 (3.03); N, 9.76 (9.52). λ_{max}/nm ($\varepsilon/M^{-1}cm^{-1}$) in dichloromethane: 422 (161500), 494 (4700), 530 (10700), 574 (41500). ^{1}H NMR (400 MHz, CDCl3) δ 9.20 (d, J = 4.5 Hz, 2H), 8.95 (d, J = 4.9 Hz, 2H), 8.80 (dd, J = 20.4, 4.7 Hz, 4H), 8.39 (t, J = 7.0 Hz, 4H), 8.11 (d, J = 8.3 Hz, 4H), 7.54 (s, 1H), 7.02 (s, 1H), 4.21 (s, 3H), 3.92 (s, 3H), 3.60 (s, 3H). ESI-MS: *m/z* = 860.6794 $[\mathbf{1}]^+$ (860.6703 calcd for $C_{42}H_{27}AuN_6O_3$) (Fig. S1).

Synthesis of 10-(4,7-dimethoxynaphthalen-1-yl)-5,15-bis(4-cyanophenyl)corrolato-Au(III), 2

A mixture of 10-(4,7-dimethoxynaphthalen-1-yl)-5,15-bis(4-cyanophenyl) corrole (0.050 gm, 0.073 mmol) and an excess of gold acetate (0.140 gm, 0.375 mmol) was dissolved in 5 mL of pyridine under stirring condition. After an hour, the solvent was evaporated and the red-brown colored crude product was subjected to column chromatography using silica gel (100-200 mesh) and dichloromethane as eluent. The desired compound was collected as a bright-red fraction. Upon recrystallization (CH_2Cl_2/hexane) pure crystalline compound, **2**, was obtained. Yield: 28% (18mg). Anal. Calcd (found) for $C_{45}H_{27}AuN_6O_2$ (**2**): C, 61.37 (61.21); H, 3.09 (3.01); N, 9.54 (9.35). λ_{max}/nm ($\varepsilon/M^{-1}cm^{-1}$) in dichloromethane: 423 (142200), 494 (3700), 533 (9300), 572 (37000). ^{1}H NMR (400 MHz, $CDCl_3$) δ 9.17 (d, J = 4.5 Hz, 2H), 8.87 (d, J = 4.9 Hz, 2H), 8.78 (d, J = 4.5 Hz, 2H), 8.64 (d, J = 4.9 Hz, 2H), 8.50 (d, J = 9.3 Hz, 1H), 8.38 (t, J = 7.4 Hz, 4H), 8.16 – 8.06 (m, 4H), 8.02 (d, J = 7.8 Hz, 1H), 7.20 – 7.07 (m, 2H), 6.40 (d, J = 2.4 Hz, 1H), 4.27 (s, 3H), 2.97 (s, 3H). ^{13}C NMR (101 MHz, $CDCl_3$) δ 158.42, 156.37, 145.35, 138.60, 136.33, 135.19, 135.16, 134.42, 133.73, 131.54, 131.10, 128.68, 128.60, 126.84, 125.93, 124.04, 120.78, 120.62, 119.24, 118.60, 116.87, 115.37, 111.73, 111.41, 107.20, 101.38, 55.92, 54.83. ESI-MS: *m/z* = 880.1810 $[\mathbf{2}]^+$ (880.1861 calcd for $C_{45}H_{27}AuN_6O_2$) (Fig. S1).

Acknowledgements

Financial support received from the Department of Atomic Energy, (India) is gratefully acknowledged. Authors thankfully acknowledge NISER, Bhubaneswar for providing infrastructure. Fonds der chemischenIndustrie (FCI) is kindly acknowledged for financial support. We are grateful to the Fonds der ChemischenIndustrie (Chemiefondsstipendium for MGS) and the Carl-Zeiss Stiftung (doctoral stipend for ND) for financial support of this work.

Notes and references

1. H. Schmidbaur, *Chem. Soc. Rev.*, 1995, **24**, 391-400.
2. S. P. Nolan, *Acc. Chem. Res.*, 2010, **44**, 91-100.
3. I. Ott, *Coord. Chem. Rev.*, 2009, **253**, 1670-1681.
4. S. P. Pricker, *Gold bulletin*, 1996, **29**, 53-60.
5. W. F. Kean, L. Hart and W. W. Buchanan, *Rheumatology*, 1997, **36**, 560-572.
6. D. A. Giljohann, D. S. Seferos, W. L. Daniel, M. D. Massich, P. C. Patel and C. A. Mirkin, *Angew. Chem. Int. Ed.*, 2010, **49**, 3280-3294.
7. A. Sigel, *Metal Ions in Biological Systems: Volume 41: Metal Ions and Their Complexes in Medication*, CRC Press, 2004.
8. T. J. Bergendahl, *J. Chem. Educ.*, 1975, **52**, 731.
9. K. M. Kadish, E. Wenbo, Z. Ou, J. Shao, P. J. Sintic, K. Ohkubo, S. Fukuzumi and M. J. Crossley, *Chem. Commun.*, 2002, 356-357.
10. R. W.-Y. Sun and C.-M. Che, *Coord. Chem. Rev.*, 2009, **253**, 1682-1691.
11. C. M. Lemon, P. J. Brothers and B. Boitrel, *Dalton Trans.*, 2011, **40**, 6591-6609.
12. A. M. Brun, A. Harriman, V. Heitz and J. P. Sauvage, *J. Am. Chem. Soc.*, 1991, **113**, 8657-8663.
13. A. M. Brun, S. J. Atherton, A. Harriman, V. Heitz and J. P. Sauvage, *J. Am. Chem. Soc.*, 1992, **114**, 4632-4639.
14. H.-Y. Liu, T.-S. Lai, L.-L. Yeung and C. K. Chang, *Org. Lett.*, 2003, **5**, 617-620.
15. R. Guilard, F. Burdet, J.-M. Barbe, C. P. Gros, E. Espinosa, J. Shao, Z. Ou, R. Zhan and K. M. Kadish, *Inorg. Chem.*, 2005, **44**, 3972-3983.
16. H.-Y. Liu, Y. Fei, Y.-T. Xie, X.-Y. Li and C. K. Chang, *J. Am. Chem. Soc.*, 2009, **131**, 12890-12891.
17. J. H. Palmer, A. C. Durrell, Z. Gross, J. R. Winkler and H. B. Gray, *J. Am. Chem. Soc.*, 2010, **132**, 9230-9231.
18. K. E. Thomas, A. B. Alemayehu, J. Conradie, C. M. Beavers and A. Ghosh, *Acc. Chem. Res.*, 2012, **45**, 1203-1214.
19. H. Zhao, K. Pierloot, E. H. G. Langner, J. C. Swarts, J. Conradie and A. Ghosh, *Inorg. Chem.*, 2012, **51**, 4002-4006.

20. C. M. Blumenfeld, R. H. Grubbs, R. A. Moats, H. B. Gray and K. Sorasaenee, *Inorg. Chem.*, 2013, **52**, 4774-4776.
21. Z. Gershman, I. Goldberg and Z. Gross, *Angew. Chem. Int. Ed.*, 2007, **46**, 4320-4324.
22. M. El Ojaimi, C. P. Gros and J.-M. Barbe, *Eur. J. Inorg. Chem.*, 2008, 1181-1186.
23. S. Kuck, G. Hoffmann, M. Broering, M. Fechtel, M. Funk and R. Wiesendanger, *J. Am. Chem. Soc.*, 2008, **130**, 14072-14073.
24. K. M. Kadish, L. Fremond, J. Shen, P. Chen, K. Ohkubo, S. Fukuzumi, M. El Ojaimi, C. P. Gros, J.-M. Barbe and R. Guilard, *Inorg. Chem.*, 2009, **48**, 2571-2582.
25. A. J. McGown, W. D. Kerber, H. Fujii and D. P. Goldberg, *J. Am. Chem. Soc.*, 2009, **131**, 8040-8048.
26. B. Gisk, F. Bregier, R. A. Krueger, M. Broering and N. Frankenberg-Dinkel, *Biochemistry*, 2010, **49**, 10042-10044.
27. M. M. Abu-Omar, *Dalton Trans.*, 2011, **40**, 3435-3444.
28. I. Nigel-Etinger, I. Goldberg and Z. Gross, *Inorg. Chem.*, 2012, **51**, 1983-1985.
29. C. I. M. Santos, E. Oliveira, J. F. B. Barata, M. A. F. Faustino, J. A. S. Cavaleiro, M. G. P. M. S. Neves and C. Lodeiro, *J. Mater. Chem.*, 2012, **22**, 13811-13819.
30. P. Leeladee, G. N. L. Jameson, M. A. Siegler, D. Kumar, S. P. de Visser and D. P. Goldberg, *Inorg. Chem.*, 2013, **52**, 4668-4682.
31. C. I. M. Santos, E. Oliveira, J. Fernandez-Lodeiro, J. F. B. Barata, S. M. Santos, M. A. F. Faustino, J. A. S. Cavaleiro, M. G. P. M. S. Neves and C. Lodeiro, *Inorg. Chem.*, 2013, **52**, 8564-8572.
32. A. Mahammed, B. Mondal, A. Rana, A. Dey and Z. Gross, *Chem. Commun.(Cambridge, U. K.)*, 2014, **50**, 2725-2727.
33. S. Nardis, D. O. Cicero, S. Licoccia, G. Pomarico, B. Berionni Berna, M. Sette, G. Ricciardi, A. Rosa, F. R. Fronczek, K. M. Smith and R. Paolesse, *Inorg. Chem.*, 2014, **53**, 4215-4227.
34. H. Furuta, H. Maeda and A. Osuka, *Chem. Commun.*, 2002, 1795-1804.
35. S. Hiroto, I. Hisaki, H. Shinokubo and A. Osuka, *Angew. Chem. Int. Ed.*, 2005, **44**, 6763-6766.
36. D. K. Dogutan, S. A. Stoian, R. McGuire Jr, M. Schwalbe, T. S. Teets and D. G. Nocera, *J. Am. Chem. Soc.*, 2010, **133**, 131-140.
37. M. Stefanelli, G. Pomarico, L. Tortora, S. Nardis, F. R. Fronczek, G. T. McCandless, K. M. Smith, M. Manowong, Y. Fang and P. Chen, *Inorg. Chem.*, 2012, **51**, 6928-6942.
38. H. L. Buckley, W. A. Chomitz, B. Koszarna, M. Tasior, D. T. Gryko, P. J. Brothers and J. Arnold, *Chem. Commun.*, 2012, **48**, 10766-10768.
39. H. L. Buckley, M. R. Anstey, D. T. Gryko and J. Arnold, *Chem. Commun.*, 2013, **49**, 3104-3106.
40. L. Yun, H. Vazquez-Lima, H. Fang, Z. Yao, G. Geisberger, C. Dietl, A. Ghosh, P. J. Brothers and X. Fu, *Inorg. Chem.*, 2014, **53**, 7047-7054.
41. A. M. Albrett, K. E. Thomas, S. Maslek, A. Młodzianowska, J. Conradie, C. M. Beavers, A. Ghosh and P. J. Brothers, *Inorg. Chem.*, 2014, **53**, 5486-5493.
42. H. L. Buckley, L. K. Rubin, M. Chromiński, B. J. McNicholas, K. H. Tsen, D. T. Gryko and J. Arnold, *Inorg. Chem.*, 2014, **53**, 7941-7950.
43. Z. Gross, N. Galili and I. Saltsman, *Angew. Chem. Int. Ed.*, 1999, **38**, 1427-1429.
44. D. Nurco and K. Smith, *Chem. Commun.*, 1999, 1307-1308.
45. B. Koszarna and D. T. Gryko, *J. Org. Chem.*, 2006, **71**, 3707-3717.
46. W. Sinha, M. G. Sommer, N. Deibel, F. Ehret, B. Sarkar and S. Kar, *Chem. Eur. J.*, 2014, **20**, 15920-15932.
47. W. Sinha, M. G. Sommer, N. Deibel, F. Ehret, M. Bauer, B. Sarkar and S. Kar, *Angew. Chem. Int. Ed.*, 2015, **54**, 13769-13774.
48. K. E. Thomas, A. B. Alemayehu, J. Conradie, C. Beavers and A. Ghosh, *Inorg. Chem.*, 2011, **50**, 12844-12851.
49. A. B. Alemayehu and A. Ghosh, *J. Porphyrins Phthalocyanines*, 2011, **15**, 106-110.
50. E. Rabinovich, I. Goldberg and Z. Gross, *Chem. Eur. J.*, 2011, **17**, 12294-12301, S12294/12291-S12294/12298.
51. Z. Ou, K. M. Kadish, J. Shao, P. J. Sintic, K. Ohkubo, S. Fukuzumi and M. J. Crossley, *Inorg. Chem.*, 2004, **43**, 2078-2086.
52. M. Krejcik, M. Danek and F. Hartl, *J. Electroanal. Chem. Interfacial Electrochem.*, 1991, **317**, 179-187.
53. G. M. Sheldrick, *Acta Crystallogr., Sect. A: Found. Crystallogr.*, 2008, **64**, 112-122.
54. P. Van der Sluis and A. Spek, *Acta Crystallogr., Sect. A: Found. Crystallogr.*, 1990, **46**, 194-201.
55. F. Neese, *Wiley Interdiscip Rev: Comput Mol Sci*, 2012, **2**, 73-78.
56. A. D. Becke, *Phys. Rev. A: At. Mol. Opt. Phys.*, 1988, **38**, 3098-3100.
57. C. Lee, W. Yang and R. G. Parr, *Phys. Rev. B: Condens. Matter*, 1988, **37**, 785-789.
58. A. D. Becke, *J. Chem. Phys.*, 1993, **98**, 5648-5652.
59. S. Grimme, J. Antony, S. Ehrlich and H. Krieg, *J. Chem. Phys.*, 2010, **132**, 154104.
60. C. van Wullen, *J. Chem. Phys.*, 1998, **109**, 392-399.
61. D. A. Pantazis, X.-Y. Chen, C. R. Landis and F. Neese, *J. Chem. Theory Comput.*, 2008, **4**, 908-919.
62. J. L. Whitten, *J. Chem. Phys.*, 1973, **58**, 4496-4501.
63. O. Vahtras, J. Almloef and M. W. Feyereisen, *Chem. Phys. Lett.*, 1993, **213**, 514-518.
64. F. Neese, *J. Comput. Chem.*, 2003, **24**, 1740-1747.
65. F. Neese, F. Wennmohs, A. Hansen and U. Becker, *Chem. Phys. Lett.*, 2009, **356**, 98-109.
66. A. Klamt and G. Schueuermann, *J. Chem. Soc., Perkin Trans. 2*, 1993, 799-805.
67. S. Sinnecker, A. Rajendran, A. Klamt, M. Diedenhofen and F. Neese, *J. Phys. Chem. A*, 2006, **110**, 2235-2245.
68. P. O. Lowdin, *J. Chem. Phys.*, 1950, **18**, 365-375.
69. S. Portmann, *CSCS/UNI Geneva: Geneva, Switzerland*, 2009.

Graphical Abstract

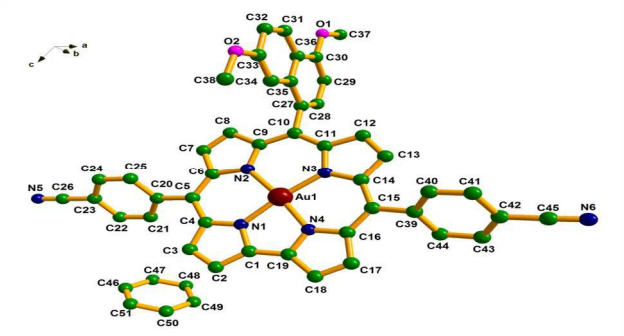

UV-vis-NIR/EPR spectroelectrochemical investigations on Au^{III} corroles display NIR electrochromism, the origins of which are all on corrole-centered processes.